

# Single PEDOT Catalyst Boosts CO<sub>2</sub> Photoreduction Efficiency

Yifan Diao, Sungyoon Jung, Mojgan Kouhnavard, Reagan Woon, Haoru Yang, Pratim Biswas,\* and Julio M. D'Arcy\*



Cite This: *ACS Cent. Sci.* 2021, 7, 1668–1675



Read Online

ACCESS |



Metrics & More

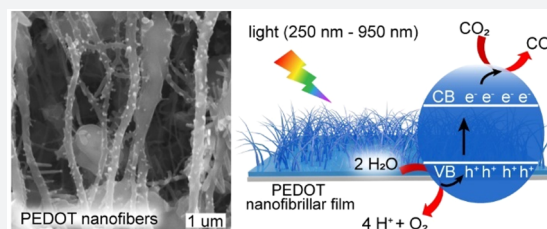


Article Recommendations



Supporting Information

**ABSTRACT:** Atmospheric pollution demands the development of solar-driven photocatalytic technologies for the conversion of CO<sub>2</sub> into a fuel; state-of-the-art cocatalyst systems demonstrate conversion efficiencies currently unattainable by a single catalyst. Here, we upend the status quo demonstrating that the nanofibrillar conducting polymer poly(3,4-ethylenedioxythiophene) (PEDOT) is a record-breaking single catalyst for the photoreduction of CO<sub>2</sub> to CO. This high catalytic efficiency stems from a highly conductive nanofibrillar structure that significantly enhances surface area, CO<sub>2</sub> adsorption and light absorption. Moreover, the polymer's band gap is optimized via chemical doping/dedoping treatments using hydrochloric acid, ammonia hydroxide, and hydrazine. The hydrazine-treated PEDOT catalyst exhibits 100% CO yield under a stable regime (>10 h) with a maximum rate of CO evolution (3000  $\mu\text{mol g}_{\text{cat}}^{-1} \text{h}^{-1}$ ) that is 2 orders of magnitude higher than the top performing single catalyst and surpassed only by three other cocatalyst systems. Nanofibrillar PEDOT provides a new direction for designing the next generation of high-efficiency photoreduction catalysts.



## INTRODUCTION

Excessive fossil fuel combustion has drastically increased net global carbon dioxide (CO<sub>2</sub>) influx into Earth's atmosphere, inducing climate change and worsening air quality, human health, and energy security.<sup>1,2</sup> The critical need for mankind to counteract increasing atmospheric greenhouse gas concentrations demands intensive research to develop processes that attenuate CO<sub>2</sub> emissions.<sup>3</sup> Photoreduction of CO<sub>2</sub> is one promising approach where abundant and sustainable solar energy is utilized, with the aid of semiconductor photocatalysts, to reduce CO<sub>2</sub> into chemical fuels.<sup>4,5</sup> In a photocatalytic system, electrons/holes generated by light absorption migrate toward catalytically active sites where they react with adsorbed CO<sub>2</sub> molecules. Catalytic efficiency relies on generation and separation of photogenerated charge carriers while minimizing recombination, as well as on efficient CO<sub>2</sub> adsorption and light absorption.<sup>6,7</sup> Numerous efforts have optimized structure and composition of photocatalysts by increasing surface area, creating surface defects on graphene, introducing nanocrystals to enhance visible light absorption and applying metal/metal oxide cocatalysts, such as Ni, TiO<sub>2</sub>, and ZnO, to facilitate charge separation. However, these cocatalysts suffer from recombination of charge carriers and band gap mismatch leading to poor conversion efficiencies.<sup>8,9</sup> As opposed to a single catalyst, delivery of photogenerated charge carriers between cocatalysts of different band gaps must overcome the high energy barrier of out-of-plane Ohmic or Schottky contact during an intramolecular cascade.<sup>10</sup> Although researchers have modified cocatalyst systems by tuning the ratio of components to precisely match the band gap, costly

fabrication techniques and low yields highlight the importance of developing a more favorable single catalyst alternative.

Among all single catalysts, conducting polymers (CPs) are a new class of organic semiconductors primed to become the next generation of multifunctional photocatalysts; this is because the  $\pi$ -conjugation backbone in CPs enhances CO<sub>2</sub> adsorption via  $\pi$ - $\pi$  interactions with delocalized p-conjugated electrons from CO<sub>2</sub> molecules. As semiconductors, CPs possess a wide light absorption range and photostability in the ultraviolet-visible-near-IR (UV-vis-NIR) region that is easily controlled by doping/dedoping treatments and further enhanced by wide-ranging nanostructures.<sup>11</sup> Growing interest in CPs has prompted recent studies on CO<sub>2</sub> photoreduction using polyaniline (PANi) and polypyrrole (PPy),<sup>12,13</sup> unfortunately the low electrical conductivity of these polymers results in low photoreduction efficiency. Poly(3,4-ethylenedioxythiophene) (PEDOT) exhibits high mobility of photogenerated electrons/holes<sup>14</sup> and is widely recognized as the most stable conductive CP (7600 S/cm) thus potentially serving as an ideal CO<sub>2</sub> photoreduction catalyst. To the best of our knowledge, there is an absence of reports in the current literature regarding its CO<sub>2</sub> photoreduction catalytic properties.

Received: June 12, 2021

Published: September 28, 2021



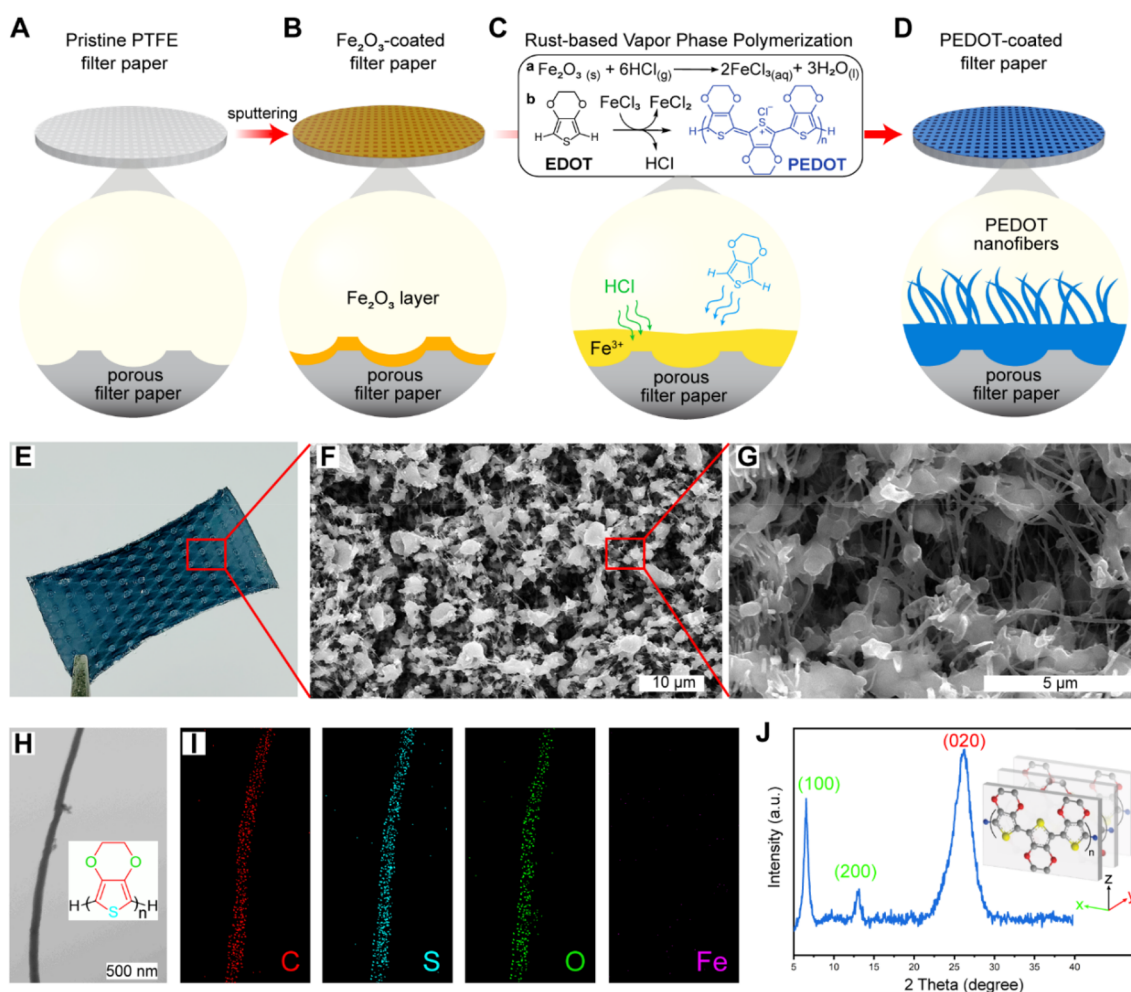


**Figure 1.** Schematic diagram of deposition of a nanofibrillar PEDOT film on a PTFE membrane and microscopic/spectroscopic characterization of a nanofibrillar PEDOT film. (A) Pristine porous PTFE membrane is (B) sputtered with a 60 nm  $\text{Fe}_2\text{O}_3$  layer. (C) Rust-based vapor phase polymerization produces PEDOT nanofibers by (a) liberating  $\text{Fe}^{3+}$  from  $\text{Fe}_2\text{O}_3$  and triggering oxidative polymerization of (b) EDOT vapor. (D) Homogeneous PEDOT nanofibrillar coating supported on a PTFE membrane. (E) Optical image of a PEDOT-coated PTFE membrane. (F) Scanning electron micrograph (SEM) shows bulk morphology of a homogeneous PEDOT coating. (G) Close-up SEM reveals the free volume architecture between nanofibers. (H) Transmission electron micrograph (TEM) of a single nanofiber (aspect ratio  $\sim 50$ ). (I) EDX maps of a nanofiber show an elemental composition consisting of C, S, O, and Fe. (J) PXRD confirms PEDOT's polycrystalline structure with three characteristic sharp peaks.

Here, for the first time, we demonstrate that a nanofibrillar PEDOT film is an ideal single catalyst for  $\text{CO}_2$  photoreduction. This film is deposited via our previously reported rust-based vapor-phase polymerization<sup>15</sup> resulting in a homogeneous PEDOT coating of high surface area possessing a nanofibrillar morphology and characterized by a high electronic conductivity (1200 S/cm). The  $\text{CO}_2$  adsorption and light absorption properties are controlled by the polymer's band gap via chemical doping and dedoping treatments using an acid (HCl) and base ( $\text{NH}_4\text{OH}$  or hydrazine), respectively. Our single catalyst results in a state-of-the-art CO yield rate ( $3000 \mu\text{mol g}^{-1} \text{h}^{-1}$ ) with 100% CO yield under stable regime ( $>10 \text{ h}$ ) representing 2 orders of magnitude higher than the best single catalyst reported and surpassed by only three other cocatalyst systems.

## RESULTS AND DISCUSSION

A conformal PEDOT nanofibrillar coating is produced via rust-based vapor-phase polymerization<sup>15</sup> by initially sputtering a 60 nm coating of  $\text{Fe}_2\text{O}_3$  oxidant precursor onto a robust

polytetrafluoroethylene (PTFE) membrane (Figure 1A). A conformally packed oxide coating exhibits a yellow color in the solid state (Figure 1B) and when dissolved, this oxide serves as an oxidizing agent promoting the deposition of a homogeneous PEDOT coating. Polymer deposition is initiated by dissolving  $\text{Fe}_2\text{O}_3$  at 140 °C using HCl vapor; dissolution liberates  $\text{Fe}^{3+}$  ions that promote organic polymerization (Figure 1C) as well as initiates inorganic hydrolysis. Monomer vapor, produced by heating a liquid EDOT reservoir, preferentially nucleates on 1-D  $\text{FeOOH}$  spindles formed during  $\text{Fe}^{3+}$  hydrolysis resulting in PEDOT nanofibers (Figure 1D). This templated vapor-phase synthetic strategy is scalable enabling deposition of a homogeneous nanofibrillar PEDOT coating on a superhydrophobic substrate.

Photocatalyst morphology, surface area, and intrinsic chemical properties are vital parameters for  $\text{CO}_2$  adsorption, light absorption, and  $\text{CO}_2$  reduction efficiency. The molecular and solid-state structure of a blue PEDOT-coated PTFE film ( $2 \text{ cm} \times 5 \text{ cm}$ ) (Figure 1E) is characterized via microscopy and spectroscopy. The polymer is uniformly integrated within

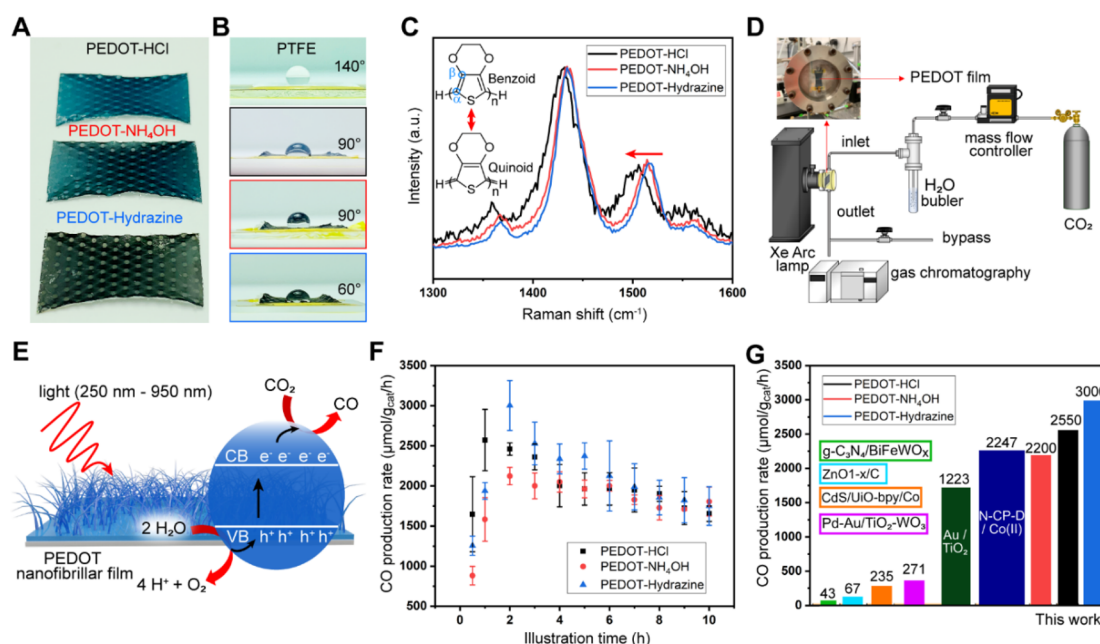


**Figure 2.** Doping/dedoping treatment of PEDOT catalyst and CO<sub>2</sub> photoreduction characterization. (A) Optical image of PEDOT-coated PTFE treated with HCl (doping), NH<sub>4</sub>OH (dedoping), and hydrazine (dedoping). (B) Contact angle data show the decreasing surface energy as a function of dedoping. (C) Raman spectra demonstrate two interchangeable polymer backbones, that is, benzoic and quinoid controlled by dedoping and doping, respectively. (D) Illustration of gas-phase CO<sub>2</sub> photoreduction setup and (E) insight process of light absorption, photogeneration and charge carrier transport. (F) Time-dependent production rates of CO versus PEDOT-HCl, PEDOT-NH<sub>4</sub>OH, and PEDOT-hydrazine catalysts under illumination (250–950 nm). (G) Our catalysts exhibit state-of-the-art performance among multiple conventional photocatalysts.

the PTFE membrane (Figure S1) and scanning electron micrographs (SEM) of low (Figures 1F and S2) and high magnification (Figure 1G) reveal a free volume web-like architecture composed of spherical aggregates interconnected by nanofibers. This open nanofibrillar structure possesses a high surface area that enhances absorption of both light and CO<sub>2</sub>; a transmission electron micrograph (TEM) shows a 100 nm mean nanofiber diameter with an aspect ratio of 50 (Figure 1H). Elemental mapping via energy-dispersive X-ray spectroscopy (Figure 1I) shows a uniform distribution and strong signals for C, O, and S corresponding to PEDOT's ethylenedioxy and thiophene ring whereas Fe signal disappears once PEDOT is purified using 6 M HCl, suggesting no Fe impurities.

Current–voltage (*I*–*V*) measurements, carried out to probe the electronic charge transport of a PEDOT film, demonstrate ohmic behavior (linear relationship) and a low resistance (large positive slope) (Figure S3) characteristic of a homogeneous and continuous percolation network that facilitates charge transport. Powder X-ray diffraction patterns (Figure 1J) further elucidate PEDOT's charge transport as a function of its polycrystalline structure. Three characteristic peaks are observed at 6.4°, 13.1°, and 26.3° corresponding to lattice planes (100), (200), and (020), respectively. The first and second planes stem from lateral chain packing (*x*-axis) and the third is due to  $\pi$ – $\pi$  stacking (*y*-axis). Low peak width values at half-height (0.4, 0.7, and 1.4) indicate a crystalline polymer structure responsible for enhanced charge transport.<sup>16</sup> Four-point probe conductivity measurements (Figure S4) show a high conductivity (1200 S/cm) stemming from the homogeneous deposition of an ordered PEDOT structure.

PEDOT's CO<sub>2</sub> adsorption capacity is enhanced by doping/dedoping treatments with acid, base, and reducing agents that

alter its surface energy.<sup>17</sup> We investigate this property utilizing HCl (37%), NH<sub>4</sub>OH (30%), and hydrazine to dope/dedope a PEDOT film resulting in PEDOT-HCl (light blue), PEDOT-NH<sub>4</sub>OH (purple), and PEDOT-hydrazine (black) (Figure 2A) samples. Contact-angle measurements are carried out to study surface energy revealing that all PEDOT coatings decrease PTFE's surface energy, while the hydrazine-treated PEDOT film exhibits the wetting degree angle at 60° (Figure 2B). PEDOT-coated membranes promote water molecule permeability confirmed by water content using TGA (Figure S5), SEM (Figure S6), and EDX (Figure S7); we suspect this is due to charged dopant effects. We gain insight into the impact of doping on chemical bonding using Raman spectroscopy. PEDOT's peak (Figure 2C) at 1357 cm<sup>-1</sup> corresponds to C <sub>$\beta$</sub> –C <sub>$\beta$</sub>  bonds, while peaks at 1437 and 1510 cm<sup>-1</sup> correspond to symmetric and asymmetric C <sub>$\alpha$</sub> =C <sub>$\beta$</sub>  stretching. The symmetric C <sub>$\alpha$</sub> =C <sub>$\beta$</sub>  stretching band shifts toward 1426 cm<sup>-1</sup> after doping with HCl.<sup>18</sup> This shift toward higher wavenumbers corresponds to greater doping levels due to an increased ratio of quinoid vs benzenoid structures in PEDOT and is consistent with previously reported behavior for other PEDOT films.<sup>19</sup>

The CO<sub>2</sub> photoreduction properties of PEDOT films are evaluated using a photoreduction analysis system under atmospheric pressure and room temperature (Figure 2D). Three initial control tests are performed to establish the source of reduction products: the first test is conducted with He as the source gas, instead of CO<sub>2</sub>, the second test is performed in the absence of PEDOT, and the third test is carried out under a lack of illumination. Carbonaceous product is absent from all three control test results demonstrating that catalysis is unfeasible in the absence of CO<sub>2</sub>, PEDOT film, or light illumination. Notably, our gas–solid interface-based photo-



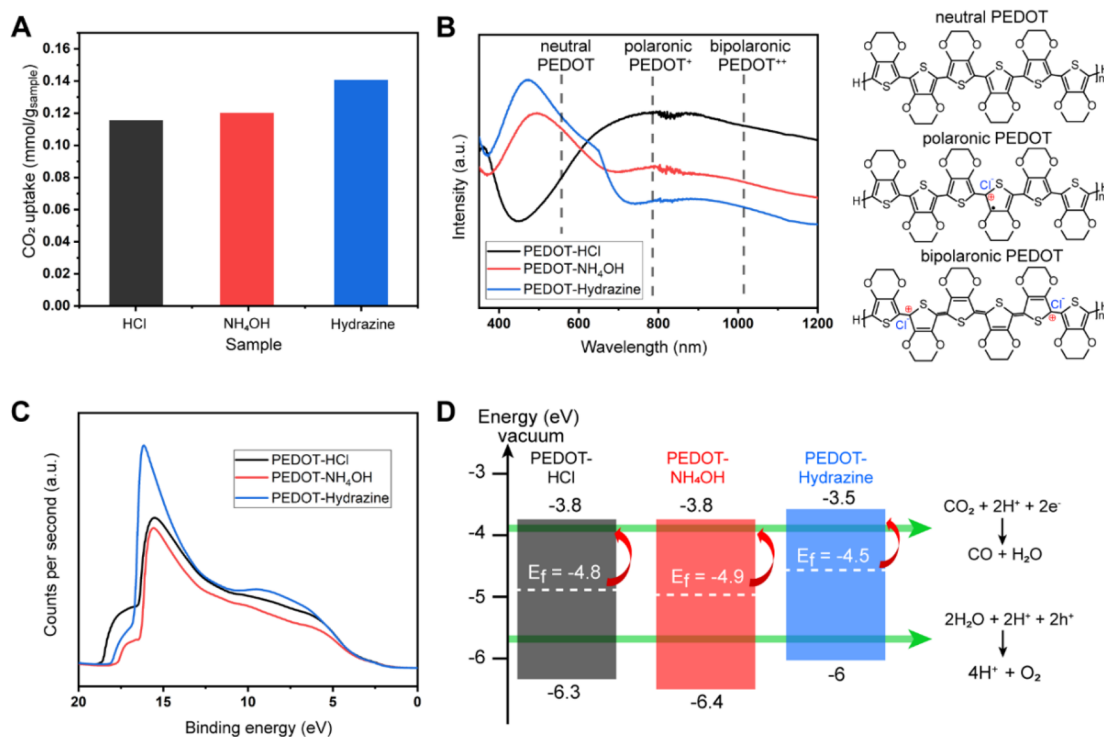


**Figure 3.** PEDOT mechanism for CO<sub>2</sub> photoreduction. (A) CO<sub>2</sub> adsorption capacity for PEDOT–HCl, PEDOT–NH<sub>4</sub>OH, and PEDOT–hydrazine catalysts at 80 °C. (B) UV–vis–NIR spectra prove that both a reducing agent and base enhance light absorption in the visible region partially converting polaronic PEDOT to its neutral state. (C) Ultraviolet photoelectron valence band spectra for PEDOT–HCl, PEDOT–NH<sub>4</sub>OH, and PEDOT–hydrazine samples predict the secondary electron edge and onset of the density of states. (D) Proposed mechanism of charge separation/transfer shows LUMO/HOMO band gaps for PEDOT–HCl, PEDOT–NH<sub>4</sub>OH, and PEDOT–hydrazine photocatalysts under a range of wavelengths (250–950 nm).

reduction system produces 100% CO as the main product because CO formation is kinetically favorable, requiring only a minimal number of electrons and protons for CO<sub>2</sub> reduction. Electrons and holes generated by UV–vis–NIR light (250–950 nm) arrive at the photoactive PEDOT film interface (active site) (Figure 2E) facilitating simultaneous reduction of CO<sub>2</sub> (electrons) and oxidation of H<sub>2</sub>O (holes). The PEDOT nanofibrillar morphology boosts light-harvesting because internal reflection of light is multiplied within the fibrillar nanostructure. Previous studies demonstrate that introducing Lewis basic sites on the surface of a catalyst enhances CO<sub>2</sub> adsorption and activation.<sup>7,35–38</sup> CO<sub>2</sub> molecules and PEDOT form electron donor–acceptor pairs because CO<sub>2</sub> possesses an electrophilic carbon attracted to lone pair electrons on a sulfur atom.<sup>29,39,40</sup> This Lewis acid–base interaction, coupled with the high surface area due to the nanofibrillar morphology of PEDOT, improves trapping and activation of CO<sub>2</sub> at the solid–gas interface with each sulfur atom serving as an active site during photoreduction. Figure 2F shows the production rates of CO using three PEDOT films as a function of illumination time, initially starting after 30 min of excitation, and reaching a maximum after one or 2 h. PEDOT–hydrazine exhibits the highest CO<sub>2</sub> photoreduction activity (3000 μmol g<sub>cat</sub><sup>−1</sup> h<sup>−1</sup>), followed by PEDOT–HCl (2550 μmol g<sub>cat</sub><sup>−1</sup> h<sup>−1</sup>) and PEDOT–NH<sub>4</sub>OH (2200 μmol g<sub>cat</sub><sup>−1</sup> h<sup>−1</sup>). Thereafter production rates gradually decrease and converge to approximately 2000 μmol g<sub>cat</sub><sup>−1</sup> h<sup>−1</sup> because of PEDOT’s photocorrosion as confirmed by UV absorption (Figure S8). To test whether Fe impurities enhance the efficiency, we compare pure PEDOT (purified) and PEDOT–FeCl<sub>2</sub> (unpurified) samples, and the result (Figure S9) suggests the

FeCl<sub>2</sub> impurities impede the reduction efficiency (decrease 70%), which might be due to the electron/hole recombination. All CO production rates decrease after reaching their maxima and remain stable for 10 h thus demonstrating excellent catalytic stability. Maximum (3000 μmol g<sub>cat</sub><sup>−1</sup> h<sup>−1</sup>) and average (2350 μmol g<sub>cat</sub><sup>−1</sup> h<sup>−1</sup>) activity rates over 10 h for the hydrazine-treated PEDOT catalyst are state-of-the-art.<sup>20,21</sup> Our performance is 2 orders of magnitude higher than the top rated single catalyst and is surpassed by only three other cocatalyst systems (Figure 2G).<sup>1,10,22–28</sup>

To study reduction rates among our catalysts, we investigate CO<sub>2</sub> adsorption, light harvesting properties and band gap structure through CO<sub>2</sub> uptake data, UV–vis–NIR and ultraviolet photoelectron spectroscopy (UPS). Adsorption of CO<sub>2</sub> on the catalytic surface is an important parameter for catalyst evaluation because it is the first step of the photocatalytic reaction. The CO<sub>2</sub> uptake data evaluated from TGA measurements (Figures 3A and S10) show the following trend: PEDOT–hydrazine (0.15) > PEDOT–NH<sub>4</sub>OH (0.113) ≈ PEDOT–HCl (0.12), confirming that low surface energy enhances CO<sub>2</sub> adsorption. The π-conjugated structure of PEDOT attracts delocalized p-conjugated electrons from CO<sub>2</sub> molecules prompting CO<sub>2</sub> uptake on catalytic surface sites.<sup>29</sup> The enhanced CO<sub>2</sub> uptake capacity exhibited by hydrazine-treated PEDOT may arise from increased interactions between quadrupolar CO<sub>2</sub> (Lewis acid) and depolarized oxygen of the ethylenedioxy ring (Lewis base) leading to greater CO<sub>2</sub> solubility and permeability in PEDOT-coated membranes.<sup>30</sup>

Another key factor for improving CO<sub>2</sub> photoreduction efficiency is light absorption because photons provide energy

for catalysis. UV–vis–NIR spectroscopy is utilized to assess charge carrier density as a function of chemical structure and characterize changes in molecular structure caused by doping. The UV–vis–NIR spectra of PEDOT (Figure 3B) is divided into three regions, that is, neutral, polaronic and bipolaronic.<sup>31,32</sup> The wavelengths chosen for CO<sub>2</sub> reduction (250–950 nm) lead to higher absorbance for dedoped PEDOT–hydrazine and PEDOT–NH<sub>4</sub>OH samples thereby promoting photogeneration of charge carriers as well as enhanced photocatalytic activity. The photothermal activity of PEDOT<sup>41,42</sup> increases in temperature during photoreduction that enhances the reaction kinetics, diffusion of CO<sub>2</sub>, and desorption of CO.<sup>2,43</sup> Larger absorbance in the polaronic and bipolaronic regions for the PEDOT–HCl sample is observed because doping ions (Cl<sup>−</sup>) help delocalization of the electron cloud thereby increasing electrical conductivity.

To understand the effect of doping on charge carrier density and mobility for enhanced CO<sub>2</sub> photoreduction, UPS is utilized for determining the valence band (VB), conduction band (CB), and Fermi level of a PEDOT catalyst (Figure 3C). Long tails in the VB spectrum of each PEDOT sample indicate different convoluted peaks and PEDOT–hydrazine in particular exhibits clear steps suggesting the presence of multiple hybridized states between VB and CB.<sup>22</sup> The work function (Fermi level energy) of PEDOT is determined by calculating the difference between the secondary electron cutoff and the energy of an incident photon. The gap between the Fermi level and the VB maximum is the onset of photoemission for valence electrons and the CB is calculated from the VB maximum, Fermi level and band gap (Figures S11–S13). An energy level diagram shows that the CB level for all PEDOT catalysts meets CO<sub>2</sub> reduction requirements by lying at potentials wider than that of CO<sub>2</sub> redox couples (Figure 3D). Hydrazine reduction dedopes PEDOT, increases its Lewis basicity, makes the photoreduction process thermodynamically more favorable (Figure 3D) and results in higher CO<sub>2</sub> adsorption thereby enhancing photocatalytic activity. PEDOT catalysts are excited by absorbing energetic photons and produce electron–hole pairs as opposed to conventional inorganic catalysts that only allow direct excitation of electrons from the VB to the CB. Further study is required to determine whether doping or dedoping changes the charge carrier density or charge carrier mobility. On the basis on our results, PEDOT–hydrazine possesses a narrower band gap requiring less excitation energy for promoting facile excitation, and the higher Fermi level also prevents the recombination process of photoexcited electrons and holes thereby facilitating photocatalytic activity.

## CONCLUSION

In summary, we present a vapor phase-deposited nanofibrillar PEDOT coating that serves as a novel single catalyst for CO<sub>2</sub> photoreduction. Our coating readily conforms to a substrate's shape and when deposited on a superhydrophobic PTFE membrane, it's characterized by high surface area and high electronic conductivity. The hydrazine-treated PEDOT catalyst demonstrates the highest CO production rate under 250–950 nm wavelengths. We achieve a state-of-the-art CO yield rate (3000 μmol g<sub>cat</sub><sup>−1</sup> h<sup>−1</sup>) with 100% CO yield under a stable regime (>10 h) surpassing the top performing single catalyst systems by 2 orders of magnitude. This work overcomes challenges associated with cocatalyst systems and opens up a new avenue for CO<sub>2</sub> photoreduction utilizing nanofibrillar

conducting polymers. Our single catalyst system represents a novel material serving as the next generation building block for developing future organic–inorganic cocatalyst systems with the potential to catapult conversion efficiencies to new levels.

## METHODS

**Materials.** Fluoropore membrane was purchased from MilliporeSigma. 3,4-ethylenedioxythiophene (EDOT, 97%), chlorobenzene (99%), hydrochloric acid (37%), ammonia hydroxide (25%), and hydrazine hydrate (50%) were purchased from Sigma-Aldrich and used as received.

**Deposition of Nanofibrillar PEDOT Film.** A solid-oxidant precursor, Fe<sub>2</sub>O<sub>3</sub>, was sputter deposited over polytetrafluoroethylene (PTFE) membrane via physical vapor deposition (Kurt J. Lesker PVD 75 RF and DC). All syntheses were performed at 140 °C for 1.5 h in glass reactors, each containing a substrate, a reservoir with 20 μL concentrated hydrochloric acid (HCl) and a reservoir with 200 μL of a 1.56 M EDOT/chlorobenzene solution. After 1.5 h, the electrodes were immediately removed from the reactors and cooled at room temperature and purified with 6 M HCl.

**PEDOT Characterization.** Scanning electron micrographs and energy-dispersive X-ray spectra were collected using a JEOL 7001LVF FE-SEM. Transmission electron micrographs were obtained using a JEOL 2100 TEM by drop-casting a dispersion of PEDOT nanofibers on a TEM grid. Raman spectra were obtained using a Renishaw inVia confocal Raman spectrometer mounted on a Leica microscope with a 20× objective and 785 nm wavelength diode laser serving as an illumination source. A low power was necessary to mitigate heating of conducting polymer samples. A Bruker d8 Advanced X-ray diffractometer was utilized to collect powder X-ray diffractograms of pulverized samples at room temperature using a Cu Kα radiation source (λ = 1.5406 Å) and LynxEye XE detector (operating at 40 kV and 40 mA); the sample holder was rotated at 30 rpm with a scan step of 0.02°. Current–voltage (*I*–*V*) curves were obtained with a built-in-house 3D printed probe station using two gold needles 1.24 mm apart. Four-point probe sheet resistance measurements were carried out using a Keithley 2450 SourceMeter with a Signatone SP4 four-point probe head.<sup>33</sup> Ultraviolet–visible–near-infrared (UV–vis–NIR) spectra were collected on a Cary 5000 UV–vis–NIR spectrophotometer. Solid PEDOT films were dispersed in HCl (37%), NH<sub>4</sub>OH, and hydrazine. X-ray photoelectron spectroscopy (XPS) was conducted on solid samples using a PHI 5000 Versaprobe II with an Al 1486.6 eV Mono-X-ray source at 51.3 W, a beam diameter of 100–200 μm and a 1 V neutralizer at 15 μA. Ultraviolet photoemission spectroscopy (UPS) measurements required a Physical Electronics 5000 VersaProbe II Scanning ESCA Microprobe and were performed to determine the valence band, conduction band and Fermi level position. He I (21.2 eV) ultraviolet source was used and a 5 V bias was applied to the sample to observe a clear secondary electron edge.

**Evaluation of PEDOT films for CO<sub>2</sub> photoreduction.** Photocatalytic activity of the synthesized PEDOT films was evaluated using a photoreduction analysis system (Figure 3D) which was discussed in our previous publications.<sup>22,34</sup> The photoreduction analysis system contains a lab-built continuous flow reactor, Xe arc lamp (Oriel 66021, Newport Co.) and gas chromatograph (GC, 6895N, Agilent Technologies, Inc.). For testing, the PEDOT film was deposited on glass and placed in a lab-built continuous flow reactor. High purity compressed

CO<sub>2</sub> was used as the source gas and its flow rate was fixed at 20 mL min<sup>-1</sup> by a mass flow controller (OMEGA engineering Inc.). The gas stream continuously passed through a water bubbler to generate a mixed flow of CO<sub>2</sub> and water vapor. Then, the mixed flow was introduced into the continuous flow reactor and a quartz window enabled positioning a sample vertically to face the light (inset photo of Figure 3E). The PEDOT film was illuminated by the Xe arc lamp, which was operated at 400 W within a UV–vis–NIR wavelength region (250–950 nm). The composition in the gas streams was continuously measured by a GC equipped with a porous layer open tubular (PLOT) capillary column (Supelco Carboxen-1010) and a thermal conductivity detector (TCD); helium was used as a carrier gas for the GC. In all experiments, the Xe arc lamp was initiated after the system was stabilized and approximately 3 mL min<sup>-1</sup> of gas were introduced to the GC. All experiments were performed at least in duplicates and no unexpected or unusually high safety hazards were encountered.

## ■ ASSOCIATED CONTENT


### SI Supporting Information

The Supporting Information is available free of charge at <https://pubs.acs.org/doi/10.1021/acscentsci.1c00712>.

Photograph of a pristine PTFE film shows macroscale morphology, scanning electron micrograph of a PEDOT nanofibrillar film, *I*–*V* curves of unpurified and purified PEDOT films (purification is carried out via repeated washes in concentrated HCl), conductivity measurement carried out using a four-point probe station, TGA of pristine PTFE and of PEDOT-coated PTFE, scanning electron micrographs of PEDOT catalysts after treatment with HCl, NH<sub>4</sub>OH, and hydrazine, energy-dispersive X-ray spectra of PEDOT catalysts after treatment with HCl, NH<sub>4</sub>OH, and hydrazine, UV–vis–NIR measurement data after CO<sub>2</sub> photoreduction, time-dependent production rates of CO versus PEDOT and PEDOT–FeCl<sub>2</sub> catalysts under illumination (250–950 nm), TGA isotherm for CO<sub>2</sub> adsorption, ultraviolet photoelectron valence band spectra for PEDOT–HCl sample predict the secondary electron edge and onset of the density of states, ultraviolet photoelectron valence band spectra for PEDOT–NH<sub>4</sub>OH sample predict the secondary electron edge and onset of the density of states, and ultraviolet photoelectron valence band spectra for PEDOT–hydrazine sample predict the secondary electron edge and onset of the density of states (PDF)

## ■ AUTHOR INFORMATION

### Corresponding Authors

**Julio M. D’Arcy** – Institute of Materials Science & Engineering and Department of Chemistry, Washington University, St. Louis, Missouri 63130, United States;  [orcid.org/0000-0002-6823-3586](https://orcid.org/0000-0002-6823-3586); Phone: (314)-935-7586; Email: [jdarcy@wustl.edu](mailto:jdarcy@wustl.edu)

**Pratim Biswas** – Institute of Materials Science & Engineering and Department of Energy, Environment & Chemical Engineering, Washington University, St. Louis, Missouri 63130, United States; Phone: (305) 284-5986; Email: [pbiswas@miami.edu](mailto:pbiswas@miami.edu)

## Authors

**Yifan Diao** – Institute of Materials Science & Engineering, Washington University, St. Louis, Missouri 63130, United States

**Sungyoon Jung** – Department of Energy, Environment & Chemical Engineering, Washington University, St. Louis, Missouri 63130, United States

**Mojgan Kouhnavard** – Department of Energy, Environment & Chemical Engineering, Washington University, St. Louis, Missouri 63130, United States

**Reagan Woon** – Department of Chemistry, Washington University, St. Louis, Missouri 63130, United States

**Haoru Yang** – Department of Chemistry, Washington University, St. Louis, Missouri 63130, United States

Complete contact information is available at:

<https://pubs.acs.org/doi/10.1021/acscentsci.1c00712>

## Author Contributions

Y.D., S.J., M.K., P.B., and J.M.D designed the experiments. Y.D., S.J., and M.K. carried out syntheses, device fabrication, characterization, and data analysis. Y.D., S.J., and M.K. analyzed data and wrote the paper. Y.D., S.J., M.K., R.W., H.Y., P.B., and J.M.D contributed to the discussion and editing of the Research Article.

## Funding

This work was supported by the financial support from the department of chemistry at Washington University.

## Notes

The authors declare no competing financial interest.

## ■ ACKNOWLEDGMENTS

We thank Dr. Huafang Li and Dr. Rahul Gupta from the Institute of Materials Science & Engineering at Washington University for help with electron microscopy and microfabrication. We are grateful to Dr. G. S. D’Arcy for editing this work.

## ■ REFERENCES

- (1) Niu, K.; Xu, Y.; Wang, H.; Ye, R.; Xin, H. L.; Lin, F.; Tian, C.; Lum, Y.; Bustillo, K. C.; Doeff, M. M.; Koper, M. T. M.; Ager, J.; Xu, R.; Zheng, H. A spongy nickel-organic CO<sub>2</sub> reduction photocatalyst for nearly 100% selective CO production. *Science Advances* **2017**, *3*, e1700921.
- (2) Thompson, W. A.; Sanchez Fernandez, E.; Maroto-Valer, M. M. Review and Analysis of CO<sub>2</sub> Photoreduction Kinetics. *ACS Sustainable Chem. Eng.* **2020**, *8* (12), 4677–4692.
- (3) Coskun, H.; Aljabour, A.; De Luna, P.; Farka, D.; Greunz, T.; Stifter, D.; Kus, M.; Zheng, X.; Liu, M.; Hassel, A. W.; Schofberger, W.; Sargent, E. H.; Sariciftci, N. S.; Stadler, P. Biofunctionalized conductive polymers enable efficient CO<sub>2</sub> electroreduction. *Science Advances* **2017**, *3*, e1700686.
- (4) Wang, Y.; Liu, X.; Han, X.; Godin, R.; Chen, J.; Zhou, W.; Jiang, C.; Thompson, J. F.; Mustafa, K. B.; Shevlin, S. A.; Durrant, J. R.; Guo, Z.; Tang, J. Unique hole-accepting carbon-dots promoting selective carbon dioxide reduction nearly 100% to methanol by pure water. *Nat. Commun.* **2020**, *11* (1), 2531.
- (5) Chen, C.; Khosrowabadi Kotyk, J. F.; Sheehan, S. W. Progress toward Commercial Application of Electrochemical Carbon Dioxide Reduction. *Chem.* **2018**, *4* (11), 2571–2586.
- (6) Wang, S.; Xu, M.; Peng, T.; Zhang, C.; Li, T.; Hussain, I.; Wang, J.; Tan, B. Porous hypercrosslinked polymer-TiO<sub>2</sub>-graphene composite photocatalysts for visible-light-driven CO<sub>2</sub> conversion. *Nat. Commun.* **2019**, *10* (1), 676.



- (7) Chang, X.; Wang, T.; Gong, J. CO<sub>2</sub> photo-reduction: insights into CO<sub>2</sub> activation and reaction on surfaces of photocatalysts. *Energy Environ. Sci.* **2016**, *9* (7), 2177–2196.
- (8) Dai, W.; Xu, H.; Yu, J.; Hu, X.; Luo, X.; Tu, X.; Yang, L. Photocatalytic reduction of CO<sub>2</sub> into methanol and ethanol over conducting polymers modified Bi<sub>2</sub>WO<sub>6</sub> microspheres under visible light. *Appl. Surf. Sci.* **2015**, *356*, 173–180.
- (9) Lee, S.; Kim, S.; Park, C.; Moon, G.-h.; Son, H.-J.; Baeg, J.-O.; Kim, W.; Choi, W. Nafion-Assisted Noncovalent Assembly of Molecular Sensitizers and Catalysts for Sustained Photoreduction of CO<sub>2</sub> to CO. *ACS Sustainable Chem. Eng.* **2020**, *8* (9), 3709–3717.
- (10) Wang, S.; Hai, X.; Ding, X.; Jin, S.; Xiang, Y.; Wang, P.; Jiang, B.; Ichihara, F.; Oshikiri, M.; Meng, X.; Li, Y.; Matsuda, W.; Ma, J.; Seki, S.; Wang, X.; Huang, H.; Wada, Y.; Chen, H.; Ye, J. Intermolecular cascaded pi-conjugation channels for electron delivery powering CO<sub>2</sub> photoreduction. *Nat. Commun.* **2020**, *11* (1), 1149.
- (11) Nai, J.; Wang, S.; Lou, X. W. Ordered colloidal clusters constructed by nanocrystals with valence for efficient CO<sub>2</sub> photo-reduction. *Science Advances* **2019**, *5*, eaax5095.
- (12) Hursan, D.; Kormanyos, A.; Rajeshwar, K.; Janaky, C. Polyaniline films photoelectrochemically reduce CO<sub>2</sub> to alcohols. *Chem. Commun. (Cambridge, U. K.)* **2016**, *52* (57), 8858–61.
- (13) Darkwah, W. K.; Teye, G. K.; Ao, Y. Graphene nanocrystals in CO<sub>2</sub> photoreduction with H<sub>2</sub>O for fuel production. *Nanoscale Advances* **2020**, *2* (3), 991–1006.
- (14) Cho, B.; Park, K. S.; Baek, J.; Oh, H. S.; Koo Lee, Y. E.; Sung, M. M. Single-crystal poly(3,4-ethylenedioxythiophene) nanowires with ultrahigh conductivity. *Nano Lett.* **2014**, *14* (6), 3321–7.
- (15) Diao, Y.; Chen, H.; Lu, Y.; Santino, L. M.; Wang, H.; D'Arcy, J. M. Converting Rust to PEDOT Nanofibers for Supercapacitors. *ACS Applied Energy Materials* **2019**, *2* (5), 3435–3444.
- (16) Diao, Y.; Lu, Y.; Yang, H.; Wang, H.; Chen, H.; D'Arcy, J. M. Direct Conversion of Fe<sub>2</sub>O<sub>3</sub> to 3D Nanofibrillar PEDOT Micro-supercapacitors. *Adv. Funct. Mater.* **2020**, *30* (32), 2003394.
- (17) Arif, M.; Barifcani, A.; Lebedev, I.; Iglauer, S. Impact of Solid Surface Energy on Wettability of CO<sub>2</sub>-brine-Mineral Systems as a Function of Pressure, Temperature and Salinity. *Energy Procedia* **2017**, *114*, 4832–4842.
- (18) Krieg, L.; Meierhofer, F.; Gorny, S.; Leis, S.; Splith, D.; Zhang, Z.; von Wenckstern, H.; Grundmann, M.; Wang, X.; Hartmann, J.; Margenfeld, C.; Mangano Clavero, I.; Avramescu, A.; Schimpke, T.; Scholz, D.; Lugauer, H. J.; Strassburg, M.; Jungclaus, J.; Bornemann, S.; Spende, H.; Waag, A.; Gleason, K. K.; Voss, T. Toward three-dimensional hybrid inorganic/organic optoelectronics based on GaN/oCVD-PEDOT structures. *Nat. Commun.* **2020**, *11* (1), 5092.
- (19) Wang, Y.; Zhu, C.; Pfattner, R.; Yan, H.; Jin, L.; Chen, S.; Molina-Lopez, F.; Lissel, F.; Liu, J.; Rabiha, N. I.; Chen, Z.; Chung, J. W.; Linder, C.; Toney, M. F.; Murmann, B.; Bao, Z. A highly stretchable, transparent, and conductive polymer. *Science Advances* **2017**, *3*, e1602076.
- (20) Di, J.; Zhu, C.; Ji, M.; Duan, M.; Long, R.; Yan, C.; Gu, K.; Xiong, J.; She, Y.; Xia, J.; Li, H.; Liu, Z. Defect-Rich Bi<sub>12</sub>O<sub>17</sub>Cl<sub>2</sub> Nanotubes Self-Accelerating Charge Separation for Boosting Photocatalytic CO<sub>2</sub> Reduction. *Angew. Chem., Int. Ed.* **2018**, *57* (45), 14847–14851.
- (21) Yu, X.; Yang, Z.; Qiu, B.; Guo, S.; Yang, P.; Yu, B.; Zhang, H.; Zhao, Y.; Yang, X.; Han, B.; Liu, Z. Eosin Y-Functionalized Conjugated Organic Polymers for Visible-Light-Driven CO<sub>2</sub> Reduction with H<sub>2</sub>O to CO with High Efficiency. *Angew. Chem., Int. Ed.* **2019**, *58* (2), 632–636.
- (22) Lin, L.-Y.; Kavadiya, S.; Karakocak, B. B.; Nie, Y.; Raliya, R.; Wang, S. T.; Berezin, M. Y.; Biswas, P. ZnO<sub>1-x</sub>/carbon dots composite hollow spheres: Facile aerosol synthesis and superior CO<sub>2</sub> photoreduction under UV, visible and near-infrared irradiation. *Appl. Catal., B* **2018**, *230*, 36–48.
- (23) Zhu, Z.; Huang, W.-R.; Chen, C.-Y.; Wu, R.-J. Preparation of Pd–Au/TiO<sub>2</sub>–WO<sub>3</sub> to enhance photoreduction of CO<sub>2</sub> to CH<sub>4</sub> and CO. *Journal of CO<sub>2</sub> Utilization* **2018**, *28*, 247–254.
- (24) Chen, C.; Wu, T.; Wu, H.; Liu, H.; Qian, Q.; Liu, Z.; Yang, G.; Han, B. Highly effective photoreduction of CO<sub>2</sub> to CO promoted by integration of CdS with molecular redox catalysts through metal-organic frameworks. *Chem. Sci.* **2018**, *9* (47), 8890–8894.
- (25) Wang, Y.; Zeng, Y.; Wan, S.; Cai, W.; Song, F.; Zhang, S.; Zhong, Q. In Situ Fabrication of 3D Octahedral g-C<sub>3</sub>N<sub>4</sub>/BiFeWO<sub>6</sub> Double-Heterojunction for Highly Selective CO<sub>2</sub> Photoreduction to CO Under Visible Light. *ChemCatChem* **2018**, *10* (20), 4578–4585.
- (26) Tahir, M. Synergistic effect in MMT-dispersed Au/TiO<sub>2</sub> monolithic nanocatalyst for plasmon-absorption and metallic inter-band transitions dynamic CO<sub>2</sub> photo-reduction to CO. *Appl. Catal., B* **2017**, *219*, 329–343.
- (27) Gao, C.; Meng, Q.; Zhao, K.; Yin, H.; Wang, D.; Guo, J.; Zhao, S.; Chang, L.; He, M.; Li, Q.; Zhao, H.; Huang, X.; Gao, Y.; Tang, Z. Co<sub>3</sub>O<sub>4</sub> Hexagonal Platelets with Controllable Facets Enabling Highly Efficient Visible-Light Photocatalytic Reduction of CO<sub>2</sub>. *Adv. Mater.* **2016**, *28* (30), 6485–90.
- (28) Zhong, W.; Sa, R.; Li, L.; He, Y.; Li, L.; Bi, J.; Zhuang, Z.; Yu, Y.; Zou, Z. A Covalent Organic Framework Bearing Single Ni Sites as a Synergistic Photocatalyst for Selective Photoreduction of CO<sub>2</sub> to CO. *J. Am. Chem. Soc.* **2019**, *141* (18), 7615–7621.
- (29) Lee, J. H.; Jung, J. P.; Jang, E.; Lee, K. B.; Hwang, Y. J.; Min, B. K.; Kim, J. H. PEDOT-PSS embedded comb copolymer membranes with improved CO<sub>2</sub> capture. *J. Membr. Sci.* **2016**, *518*, 21–30.
- (30) Hong, J. Y.; Huh, S. Hollow S-doped carbon spheres from spherical CT/PEDOT composite particles and their CO<sub>2</sub> sorption properties. *J. Colloid Interface Sci.* **2014**, *436*, 77–82.
- (31) Perry, S. C.; Pangotra, D.; Vieira, L.; Csepei, L.-I.; Sieber, V.; Wang, L.; Ponce de León, C.; Walsh, F. C. Electrochemical synthesis of hydrogen peroxide from water and oxygen. *Nature Reviews Chemistry* **2019**, *3* (7), 442–458.
- (32) Zozoulenko, I.; Singh, A.; Singh, S. K.; Gueskine, V.; Crispin, X.; Berggren, M. Polarons, Bipolarons, And Absorption Spectroscopy of PEDOT. *ACS Applied Polymer Materials* **2019**, *1* (1), 83–94.
- (33) Lu, Y.; Santino, L. M.; Acharya, S.; Anandarajah, H.; D'Arcy, J. M. Studying Electrical Conductivity Using a 3D Printed Four-Point Probe Station. *J. Chem. Educ.* **2017**, *94* (7), 950–955.
- (34) Wang, W.-N.; Park, J.; Biswas, P. Rapid synthesis of nanostructured Cu–TiO<sub>2</sub>–SiO<sub>2</sub> composites for CO<sub>2</sub> photoreduction by evaporation driven self-assembly. *Catal. Sci. Technol.* **2011**, *1* (4), 593.
- (35) Freund, H.-J.; Roberts, M. W. Surface Chemistry of Carbon Dioxide. *Surf. Sci. Rep.* **1996**, *25* (8), 225–273.
- (36) Xie, S.; Wang, Y.; Zhang, Q.; Deng, W.; Wang, Y. MgO- and Pt-Promoted TiO<sub>2</sub> as an Efficient Photocatalyst for the Preferential Reduction of Carbon Dioxide in the Presence of Water. *ACS Catal.* **2014**, *4* (10), 3644–3653.
- (37) Meng, X.; Ouyang, S.; Kako, T.; Li, P.; Yu, Q.; Wang, T.; Ye, J. Photocatalytic CO<sub>2</sub> Conversion over Alkali Modified TiO<sub>2</sub> without Loading Noble Metal Cocatalyst. *Chem. Commun.* **2014**, *50* (78), 11517–11519.
- (38) Xie, S.; Wang, Y.; Zhang, Q.; Fan, W.; Deng, W.; Wang, Y. Photocatalytic Reduction of CO<sub>2</sub> with H<sub>2</sub>O: Significant Enhancement of the Activity of Pt–TiO<sub>2</sub> in CH<sub>4</sub> Formation by Addition of MgO. *Chem. Commun.* **2013**, *49* (24), 2451–2453.
- (39) Seema, H.; Kemp, K. C.; Le, N. H.; Park, S.-W.; Chandra, V.; Lee, J. W.; Kim, K. S. Highly Selective CO<sub>2</sub> Capture by S-Doped Microporous Carbon Materials. *Carbon* **2014**, *66*, 320–326.
- (40) Kundu, S. K.; Bhaumik, A. Novel Nitrogen and Sulfur Rich Hyper-Cross-Linked Microporous Poly-Triazine-Thiophene Copolymer for Superior CO<sub>2</sub> Capture. *ACS Sustain. ACS Sustainable Chem. Eng.* **2016**, *4* (7), 3697–3703.
- (41) Jeong, C. J.; Sharker, S. M.; In, I.; Park, S. Y. Iron Oxide@PEDOT-Based Recyclable Photothermal Nanoparticles with Poly-(Vinylpyrrolidone) Sulfobetaines for Rapid and Effective Antibacterial Activity. *ACS Appl. Mater. Interfaces* **2015**, *7* (18), 9469–9478.
- (42) Liu, D.; Ma, L.; An, Y.; Li, Y.; Liu, Y.; Wang, L.; Guo, J.; Wang, J.; Zhou, J. Thermoresponsive Nanogel-Encapsulated PEDOT and

HSP70 Inhibitor for Improving the Depth of the Photothermal Therapeutic Effect. *Adv. Funct. Mater.* **2016**, 26 (26), 4749–4759.

(43) Lee, J.; Sorescu, D. C.; Deng, X.; Jordan, K. D. Diffusion of CO<sub>2</sub> on the Rutile TiO<sub>2</sub>(110) Surface. *J. Phys. Chem. Lett.* **2011**, 2 (24), 3114–3117.